

Nonequilibrium Phase Transitions in Repulsive Binary Mixtures

Pedro Antonio Santos-Flórez¹ and Maurice de Koning^{1,2,*}

¹*Instituto de Física "Gleb Wataghin", Universidade Estadual de Campinas, UNICAMP, 13083-859, Campinas, São Paulo, Brazil*

²*Center for Computing in Engineering & Sciences, Universidade Estadual de Campinas, UNICAMP, 13083-861, Campinas, São Paulo, Brazil*

(Dated: September 3, 2022)

We consider nonequilibrium phase transitions in classical binary mixtures described by a set of different purely repulsive pair interaction potentials during which an infinite-temperature homogeneous initial phase is instantaneously quenched to zero temperature. It is found that such systems display two kinds of second-order nonequilibrium transition, corresponding to either a conserved or non-conserved order parameter. The type can be controlled by tuning the interactions between unlike particles, with strong inter-species repulsion leading to unmixing, and weak repulsion giving rise to a continuous crystallization process that is barrier-less and produces scale-invariant crystal grain-size distributions. Furthermore, the behavior of the potential-energy function in the neighborhood of zero separation is directly related to the propensity of the continuous ordering transition.

Classical systems described by repulsive pair potentials have been the subject of intense investigation for over five decades [1–31]. Not in the least due to their role as effective descriptions for interactions in soft-condensed-matter systems [32–42], substantial effort has been directed towards elucidating the equilibrium phase behavior of such models, considering both single-component samples as well as multi-component mixtures [17–31]. Nonequilibrium phenomena, on the other hand, have received much less attention, despite their key role in self-organization phenomena in such systems [43–53]. Indeed, one of the challenges in soft-matter materials design concerns the ability to adjust the effective interaction parameters so as to control the self-organization process and achieve desired self-assembled structures [53].

In this context, processes that display spontaneous development of structure from an initially disordered state [43, 52, 53] are of particular interest. A typical example is a process in which a high-temperature, homogeneous phase evolves upon a sudden deep quench into a low-temperature state. Considering mixtures, the spontaneous decay of such an initially unstable phase can occur by means of two types of second-order nonequilibrium phase transition, depending on whether the involved order parameter is conserved or non-conserved [54, 55], respectively. The prototypical example of the first kind are unmixing transitions in which the conserved order parameter is related to composition. The second kind concerns spontaneous ordering transformations in which a non-conserved order parameter, for instance related to structural quantities such as crystal symmetry and/or orientation [54, 55], is relevant. While fluid-fluid unmixing transitions proceeding are quite common for the class of repulsive pair potentials [41, 56, 57], the occurrence of continuous ordering phenomena in such systems has so far not been observed. In fact, to the best of our knowledge, spontaneous ordering transitions have so far only been observed for spin systems such as the Ising

model [55], while there have been no reports for model systems characterized by continuous interactions. Above all, to date there are no known model systems that display both types of transition, depending on boundary conditions and/or model parameters.

In this Letter we show that symmetric binary mixtures described by a variety of purely repulsive pairwise interactions display both kinds of second-order nonequilibrium transition and that the observed type can be controlled by tuning the interactions between unlike particles. While strong inter-species repulsion gives rise to unmixing, weak values lead to a spontaneous development of crystalline order, forming a polycrystalline solid of uniform composition. However, unlike common first-order freezing transitions, this crystallization process is continuous in nature in that it is barrier-less and gives rise to scale-invariant grain-size distributions. Furthermore, we find that the behavior of the potential-energy function in the neighborhood of zero separation is directly related to the propensity of the continuous ordering transition.

All our results are based on simulations of nonequilibrium processes in which a random initial configuration is quenched to its corresponding local minimum on the potential-energy landscape (PEL) [59–61], mimicking a process in which an infinite-temperature state is quenched to zero temperature infinitely rapidly. This process is implemented computationally in the following way. First, for a specified particle density, we construct a cubic, periodic simulation cell with a volume V that corresponds to a given total particle number N . Subsequently, the system is initialized by randomly placing the N particles in the cell, giving rise to a structureless, uniform position distribution. Finally, a conjugate-gradient (CG) minimization is invoked to locate its associated inherent structure on the PEL. All the CG calculations have been performed using the Polak-Ribiere version of the CG algorithm as implemented in the LAMMPS package [62], using as a stopping criterion a tolerance value of

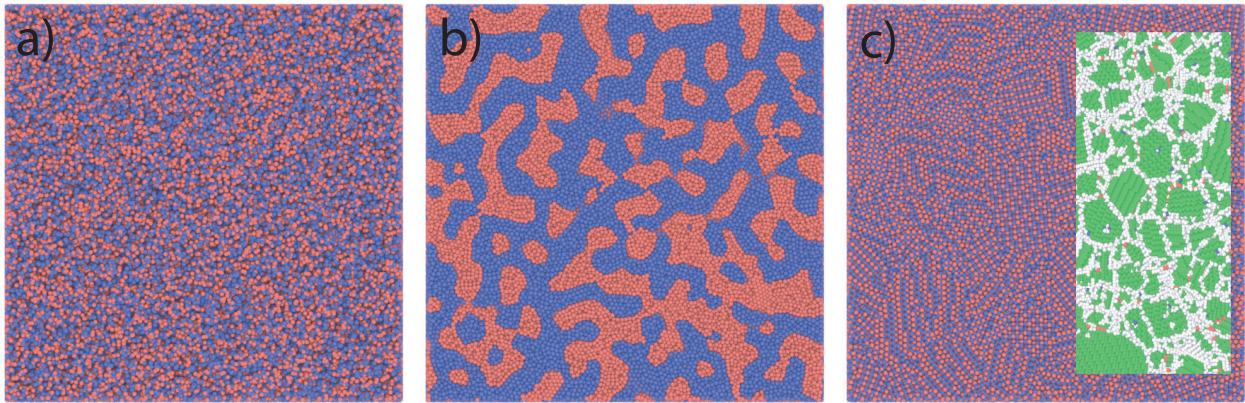


Figure 1. (Color online) Typical configurations containing $N = 10^7$ particles, with the distinct species shown in blue and red, respectively, as obtained from the CG quench protocol for the symmetrical binary UF model for two different values for the inter-species interaction energy scale. a) Random initial configuration. b) Phase-separating system for strong inter-species repulsion. c) Spontaneous ordering into a rock-salt (B1) type polycrystal of uniform composition. Inset displays part of the grain structure, showing only the A -type particles and coloring the particles according to local crystal symmetry [58], with the green, red, blue particles locally being in an fcc, hcp and bcc arrangement, respectively, and the white particles representing those in the disordered surroundings of the grain boundaries.

$10^{-4} \epsilon/\sigma$ for the 2-norm of the $3N$ -dimensional total-force vector.

As a first case we consider a binary mixture with inter-particle interactions described by the Uhlenbeck-Ford (UF) model [63–66], which is characterized by a logarithmic divergence at zero separation and belongs to the class of so-called ultrasoft potentials [36]. Specifically, the UF model is defined by the potential-energy function $u(r_{ij}) = -\epsilon_{ij} \ln(1 - e^{-r_{ij}^2/\sigma_{ij}^2})$, where ϵ_{ij} and σ_{ij} are energy and length scales associated with the interactions between particles i and j , and r_{ij} is the distance between them. We fix the energy scales of the interactions between particles of the same species to be $\epsilon_{AA} = 100\epsilon$ and $\epsilon_{BB} = 200\epsilon$, respectively, whereas the energy scale ϵ_{AB} for interactions between A and B particles is variable. The length scale is chosen to be the same for all interaction types, i.e., $\sigma_{AA} = \sigma_{BB} = \sigma_{AB} = \sigma$ and the cut-off for the interaction calculation is set at $r_c = 4\sigma$.

Fig. 1 displays typical configurations obtained for the UF mixture at a reduced particle density $\rho^* \equiv N\sigma^3/V = 1$. Fig. 1 a) depicts a random arrangement that serves as an infinite-temperature initial condition, whereas Figs. 1b) and c) show snapshots after CG minimization for two different values of the inter-species interaction parameter, ϵ_{AB} . The former portrays a case of strong inter-species repulsion at $\epsilon_{AB} = 175\epsilon$, for which the system is manifestly unstable with respect to composition fluctuations [67], leading to an unmixing transition that constitutes an example of the first type of continuous nonequilibrium transition discussed above involving a conserved order parameter. For a weak inter-species interaction at $\epsilon_{AB} = 20\epsilon$, on the other hand, the instability is fundamentally different, as can be seen in Fig. 1c). The sys-

tem remains uniform with respect to composition, but instead spontaneously develops crystalline order, reaching an inherent structure featuring a polycrystal composed of grains with the rock-salt (B1) structure, which consists of two interpenetrating fcc lattices, each occupied by either A or B . This grain structure can be discerned more clearly by visualizing only one of the two species, as has been done in the inset of Fig. 1c). These results do not depend on the particular initial condition. Indeed, when starting from the same initial condition, one obtains an unmixed final configuration for $\epsilon_{AB} = 175\epsilon$ and a polycrystalline structure for $\epsilon_{AB} = 20\epsilon$.

Interestingly, the nature of this crystallization process is fundamentally different from the usual first-order character of freezing phenomena observed under conditions of thermodynamic equilibrium. Instead, it is an example of the second type of continuous nonequilibrium transition discussed above, involving a nonconserved order parameter which, in this case, describes the degree of crystallinity. The evidence for the continuous nature of this nonequilibrium freezing transition is two-fold. First, there is no energy barrier between the structureless initial configuration and the final polycrystalline structure since they are connected by a CG sequence. This is the main difference compared to first-order transitions, for which initial and final configurations are separated by an energy barrier that cannot be surmounted using minimization techniques such as CG. Second, the grain-size distribution of the polycrystalline structure displays scale-free features that are characteristic for continuous phase transitions [68]. To verify this we analyze the final configuration from a CG minimization for a cell containing $N = 10^7$ particles with $\epsilon_{AB} = 20\epsilon$ and employ the

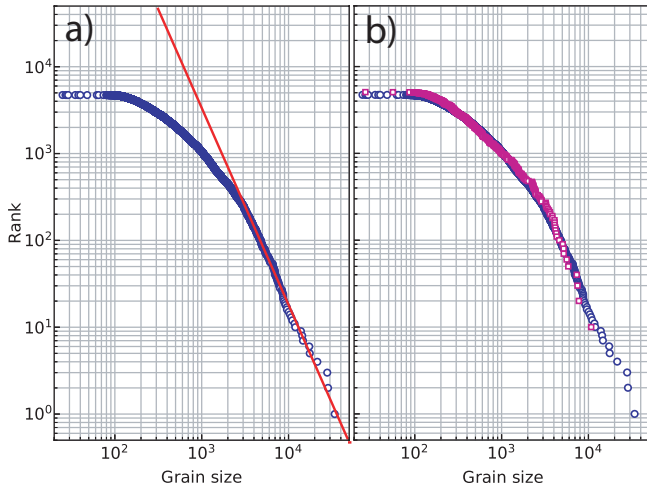


Figure 2. (Color online) a) Log-log graph of rank-size representation for A-type grain size distribution, plotting the rank of each grain in terms of its size as a function of grain size, such that the largest and smallest grains are ranked first and last, respectively. Blue circles depict results obtained for cell containing 10^7 particles. Red line represents a guide to the eye, obtained by a linear fit to the data for the 125 largest grains. b) Comparison between rank-size plots for 10^7 (blue circles) and 10^6 (magenta squares) cells. Rank data for the 10^6 cell have been multiplied by a factor 10.

recently developed grain-tracking algorithm (GTA) [69] to identify individual grains and determine their sizes in terms of particle numbers [67]. Fig. 2b) shows a log-log rank-size representation [68, 70] of the grain size distribution for the A-type sublattice, in which the rank of each grain in terms of its size is plotted as a function of grain size, such that the largest and smallest grains are ranked first and last, respectively. The graph clearly displays a linear regime for grain sizes larger than ~ 4000 particles, indicating that, asymptotically, the distribution for the grain size k follows a power law of the form $p(k) \sim k^{-\alpha}$, with an exponent $\alpha = 3.3 \pm 0.2$. The results obtained for the B-type sublattice are statistically identical [67]. The power-law dependence indicates that the grain-size distribution is scale free, meaning that it looks the same regardless of the scale at which one looks at it [68]. To verify possible system size effects we carry out the CG procedure for a cell ten times smaller, containing 10^6 particles. Fig. 2b) compares the rank-size results for both system sizes, where the rank data for the 10^6 -particle system have been multiplied by 10 to enable a direct comparison with distribution obtained for the 10^7 -particle cell. Both distributions essentially overlap, indicating that the obtained grain-size distribution for the considered system size is robust.

As evidenced in Fig. 1, the magnitude of the interspecies interaction strength ϵ_{AB} determines the type of

transition that occurs. To further analyze this influence we carry out a series of quench CG simulations for a set of ϵ_{AB} -values between 0 and 200ϵ , employing cells containing of the order of $10^3 - 10^4$ particles. In addition, we also investigate the possible role of the particle-number density by considering a range of ρ^* -values for each ϵ_{AB} . To automate the detection of the phase transitions we monitor the displacements of the particles during each quench simulation, comparing their positions in the initially structureless state to those at the end of the CG minimization procedure. Fig. 3a) displays a density plot of the mean particle displacement for the UF system, measured in units of the average particle separation $d \equiv \rho^{*-1/3}$, as a function of ϵ_{AB} and ρ^* . It displays three well-defined regimes, characterized by distinct values for the mean particle displacement. The yellow band on the left corresponds to values of the order of $1-2d$ and signals the instability of the random initial configuration that leads to its decay into the self-similar rock-salt structure through the continuous ordering transition. The mostly blue band on the right corresponds to the instability that gives rise to the unmixing transition in which particles move over much larger distances. Finally, in the orange-colored areas the displacements are less than the average particle separation, meaning that the initial configurations are metastable, i.e., they are “close” to their corresponding local minima, which retain their homogeneous and amorphous character. A further notable characteristic is that the identification of these 3 groups involves ϵ_{AB} only, being essentially independent of ρ^* , except for very low values for which the distances between the particles become large and the interactions between them weak. This implies that the basin-structure of the PEL-part associated with high-temperature configurations is invariant with respect to uniform volume scaling [60].

The observed phenomena are not limited to the binary UF system and also occur for other types of purely-repulsive interaction types. This is illustrated in Figs. 3 b-e), which depict density plots of the mean particle distance for the inverse fourth-power law (IPL4), the inverse sixth-power law (IPL6), the Weeks-Chandler-Andersen (WCA) and the Gaussian core (GC) models [67], respectively. For all these systems the same 3 regimes can be identified, observing unmixed structures for large values for ϵ_{AB} , continuous ordering transitions to rock-salt-type polycrystals for weak interspecies interactions and amorphous inherent structures in between. A particularly interesting issue concerns the relation between the continuous ordering regime and the functional form of the repulsive interaction. Specifically, the shape and the extent of the continuous ordering region is seen to correlate with the rate at which the potential-energy function diverges at the origin. Along the sequence shown in Fig. 3 a) to d), in which the divergence change from slow (logarithmic) to fast (r^{-12}), the range of energy scales ϵ_{AB} for which continuous crystallization occurs re-

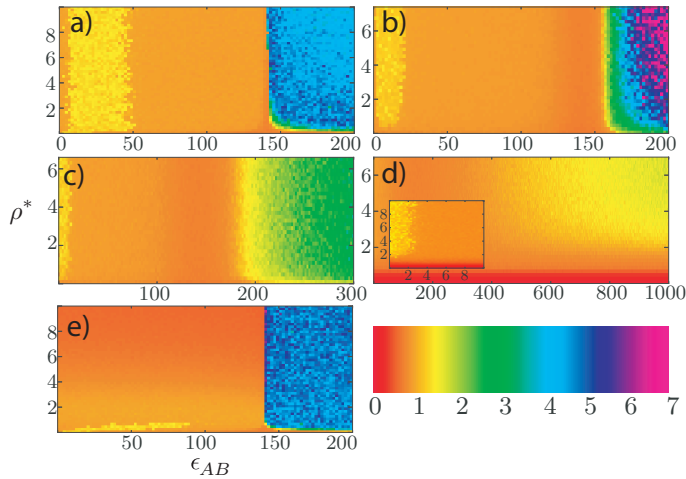


Figure 3. (Color online) Density plots of mean particle displacement in units of the mean interparticle distance $d \equiv \rho^*{}^{-1/3}$ during CG quench as a function of the interaction energy scale ϵ_{AB} and the reduced density ρ^* for the UF model (a), the IPL4 (b), IPL6 (c), WCA (d) and GC (e) potentials. Inset in (d) shows zoom into region with $\epsilon_{AB} < 10\epsilon$. Colors defined in the color bar distinguish between different displacement magnitudes.

duces systematically. Indeed, the role of the behavior of the pair potential at the origin in the ordering transition becomes even more evident when considering the GC force field, which does not diverge at the origin, tending to a constant value and zero derivative [67]. As shown in Fig. 3 e), the ordering transition to the rock-salt polycrystal structure is now restricted to a very narrow region in the $\epsilon_{AB} - \rho^*$ plane, disappearing altogether for densities above ~ 0.8 .

In summary, we show that classical symmetric binary mixtures of particles interacting through purely repulsive forces display both kinds of nonequilibrium phase transition, characterized by either a conserved or non-conserved order parameter, upon rapidly quenching an infinite-temperature initial structure to zero temperature. The observed type of transition can be controlled by tuning the interactions between unlike particles, with strong inter-species repulsion giving rise to unmixing, whereas weak interactions lead to a spontaneous development of crystalline order, forming a rock-salt-type polycrystalline solid of uniform composition. Unlike common first-order transitions this crystallization process is continuous in nature and its propensity correlates with the behavior of the potential-energy function in the neighborhood of zero separation.

We gratefully acknowledge support from the Brazilian agencies CNPq, Capes, Fapesp 2016/23891-6 and the Center for Computing in Engineering & Sciences - Fapesp/Cepid no. 2013/08293-7. Part of the calculations were performed at CCJDR-IFGW-UNICAMP. The authors acknowledge the National Laboratory for Sci-

entific Computing (LNCC/MCTI, Brazil) for providing HPC resources of the SDumont supercomputer, which have contributed to the research results reported in this paper. URL: <http://sdumont.lncc.br>

* dekonig@ifi.unicamp.br

- [1] F. H. Stillinger and E. Helfand, *J. Chem. Phys.* **41**, 2495 (1964).
- [2] E. Helfand and F. H. Stillinger, *J. Chem. Phys.* **49**, 1232 (1968).
- [3] A. Baram, *J. Phys. A* **16**, L19 (1983).
- [4] A. Baram and J. S. Rowlinson, *J. Phys. A* **23**, L399 (1990).
- [5] A. Baram and J. S. Rowlinson, *Mol. Phys.* **74**, 707 (1991).
- [6] A. Baram, M. Maddox, and J. S. Rowlinson, *Mol. Phys.* **76**, 1093 (1992).
- [7] A. Baram, M. Maddox, and J. S. Rowlinson, *Mol. Phys.* **79**, 589 (1993).
- [8] M. Dijkstra and R. van Roij, *J. Phys.: Condens. Matter* **10**, 1219 (1998).
- [9] A. Lang, C. N. Likos, M. Watzlawek, and H. Löwen, *J. Phys.: Condens. Matter* **12**, 5087 (2000).
- [10] A. A. Louis, P. G. Bolhuis, and J. P. Hansen, *Phys. Rev. E* **62**, 7961 (2000).
- [11] R. J. Speedy, *J. Phys.: Condens. Matter* **15**, S1243 (2003).
- [12] G. Cinacchi, Y. Martínez-Ratón, L. Mederos, G. Navascués, A. Tani, and E. Velasco, *J. Chem. Phys.* **127**, 214501 (2007).
- [13] M. A. Glaser, G. M. Grason, R. D. Kamien, A. Košmrlj, C. D. Santangelo, and P. Ziherl, *EPL* **78**, 46004 (2007).
- [14] F. Saija, S. Prestipino, and G. Malescio, *Phys. Rev. E* **80**, 031502 (2009).
- [15] L. Berthier, E. Flenner, H. Jacquin, and G. Szamel, *Phys. Rev. E* **81**, 031505 (2010).
- [16] M. Schmiedeberg, T. K. Haxton, S. R. Nagel, and A. J. Liu, *EPL* **96**, 36010 (2011).
- [17] J. Russo and H. Tanaka, *Soft Matter* **8**, 4206 (2012).
- [18] A. Travesset, *Proc Natl Acad Sci USA* (2015).
- [19] N. Horst and A. Travesset, *J. Chem. Phys.* **144**, 014502 (2016).
- [20] F. H. Stillinger, *J. Chem. Phys.* **65**, 3968 (1976).
- [21] P. Hansen, J., D. Goulding, and R. van Roij, *J. Phys. IV France* **10**, Pr5 (2000).
- [22] S. Prestipino, F. Saija, and P. V. Giaquinta, *J. Chem. Phys.* **123**, 144110 (2005).
- [23] S. Prestipino, F. Saija, and P. V. Giaquinta, *Phys. Rev. E* **71**, 050102(R) (2005).
- [24] G. Malescio and G. Pellicane, *Nature Materials* **2**, 97 (2003).
- [25] B. M. Mladek, D. Gottwald, G. Kahl, M. Neumann, and C. N. Likos, *Phys. Rev. Lett.* **96**, 045701 (2006).
- [26] C. N. Likos, B. M. Mladek, D. Gottwald, and G. Kahl, *J. Chem. Phys.* **126**, 224502 (2007).
- [27] C. N. Likos, B. M. Mladek, A. J. Moreno, D. Gottwald, and G. Kahl, *Comput. Phys. Commun.* **179**, 71 (2008).
- [28] S. D. Overduin and C. N. Likos, *EPL* **85**, 26003 (2009).
- [29] A. J. Archer, C. N. Likos, and R. Evans, *J. Phys.: Condens. Matter* **16**, L297 (2004).
- [30] H. Shin, G. M. Grason, and C. D. Santangelo, *Soft Mat-*

- ter **5**, 3629 (2009).
- [31] L. A. Shall and S. A. Egorov, *J. Chem. Phys.* **132**, 184504 (2010).
- [32] C. N. Likos, H. Löwen, M. Watzlawek, B. Abbas, O. Jucknischke, J. Allgaier, and D. Richter, *Phys. Rev. Lett.* **80**, 4450 (1998).
- [33] M. Watzlawek, C. N. Likos, and H. Löwen, *Phys. Rev. Lett.* **82**, 5289 (1999).
- [34] C. von Ferber, A. Jusufi, M. Watzlawek, C. N. Likos, and H. Löwen, *Phys. Rev. E* **62**, 6949 (2000).
- [35] C. N. Likos, *Phys. Rep.* **348**, 267 (2001).
- [36] C. N. Likos, N. Hoffmann, H. Löwen, and A. A. Louis, *J. Phys.: Condens. Matter* **14**, 7681 (2002).
- [37] C. N. Likos, *Soft Matter* **2**, 478 (2006).
- [38] C. Mayer, E. Zaccarelli, E. Stiakakis, C. N. Likos, F. Sciortino, A. Munam, M. Gauthier, N. Hadjichristidis, H. Iatrou, P. Tartaglia, H. Lowen, and D. Vlassopoulos, *Nat. Mater.* **7**, 780 (2008).
- [39] B. M. Mladek, G. Kahl, and C. N. Likos, *Phys. Rev. Lett.* **100**, 028301 (2008).
- [40] C. Mayer, F. Sciortino, C. N. Likos, P. Tartaglia, H. Löwen, and E. Zaccarelli, *Macromolecules* **42**, 423 (2009).
- [41] M. Camargo and C. N. Likos, *Mol. Phys.* **109**, 1121 (2011).
- [42] A. Nikoubashman, N. A. Mahynski, B. Capone, A. Z. Panagiotopoulos, and C. N. Likos, *J. Chem. Phys.* **143**, 243108 (2015).
- [43] G. Nicolis and I. Prigogine, *Self-Organization in Nonequilibrium Systems: From Dissipative Structures to Order Through Fluctuations* (Wiley, 1977).
- [44] T. A. Witten, *Rev. Mod. Phys.* **71**, S367 (1999).
- [45] R. L. Marson, C. L. Phillips, J. A. Anderson, and S. C. Glotzer, *Nano Lett.* **14**, 2071 (2014).
- [46] A. M. Kalsin, M. Fialkowski, M. Paszewski, S. K. Smoukov, K. J. M. Bishop, and B. A. Grzybowski, *Science* **312**, 420 (2006).
- [47] W. L. Miller and A. Cacciuto, *Phys. Rev. E* **80**, 021404 (2009).
- [48] X. Ye, C. Zhu, P. Ercius, S. N. Raja, B. He, M. R. Jones, M. R. Hauwiller, Y. Liu, T. Xu, and A. P. Alivisatos, *Nature Communications* **6**, 10052 (2015).
- [49] A. Kumar and V. Molinero, *J. Phys. Chem. Lett.* **8**, 5053 (2017).
- [50] X. Ye, J. Chen, and C. B. Murray, *J. Am. Chem. Soc.* **133**, 2613 (2011).
- [51] R. J. Macfarlane, B. Lee, M. R. Jones, N. Harris, G. C. Schatz, and C. A. Mirkin, *Science* **334**, 204 (2011).
- [52] C. Knorowski, S. Burleigh, and A. Travesset, *Phys. Rev. Lett.* **106**, 215501 (2011).
- [53] C. Knorowski and A. Travesset, *Curr. Opin. Solid State Mater. Sci.* **15**, 262 (2011).
- [54] R. Balluffi, S. Allen, W. Carter, and R. Kemper, *Kinetics Of Materials* (J. Wiley & Sons, 2005) pp. –.
- [55] M. Henkel and M. Pleimling, *Non-Equilibrium Phase Transitions: Volume 2: Ageing and Dynamical Scaling Far from Equilibrium* (Springer Netherlands, 2011).
- [56] A. J. Archer and R. Evans, *Phys. Rev. E* **64**, 041501 (2001).
- [57] S. Kambayashi and Y. Hiwatari, *Phys. Rev. A* **46**, 1014 (1992).
- [58] A. Stukowski, *Model. Simul. Mater. Sci. Eng.* **18**, 015012 (2010).
- [59] F. H. Stillinger, *Science* **267**, 1935 (1995).
- [60] F. Stillinger, *Energy Landscapes, Inherent Structures, and Condensed-Matter Phenomena* (Princeton University Press, 2015).
- [61] D. J. Wales, *Energy Landscapes: Applications to Clusters, Biomolecules and Glasses* (Cambridge University Press, 2003).
- [62] S. Plimpton, *J. Comput. Phys.* **117**, 1 (1995).
- [63] G. Uhlenbeck and G. Ford, “Studies in statistical mechanics,” in *Series in physics*, v. 1, edited by J. de Boer and G. Uhlenbeck (North-Holland Publishing Company, 1962) Chap. The development of linear graphs with applications to the theory of the virial development of the properties of gases, p. 182.
- [64] R. Paula Leite, R. Freitas, R. Azevedo, and M. de Koning, *J. Chem. Phys.* **145**, 194101 (2016).
- [65] R. Paula Leite, P. A. Santos-Flórez, and M. de Koning, *Phys. Rev. E* **96**, 032115 (2017).
- [66] R. Paula Leite and M. de Koning, *Comput. Mater. Sci.* **159**, 316 (2019).
- [67] For further details, see Supplemental Material.
- [68] M. Newman, *Contemp. Phys.* **46**, 323 (2005).
- [69] J. F. Panzarino and T. J. Rupert, *JOM* **66**, 417 (2014).
- [70] A. Clauset, C. Shalizi, and M. Newman, *SIAM Rev.* **51**, 661 (2009).

Supplemental Material for “Nonequilibrium Phase Transitions in Repulsive Binary Mixtures”

Pedro Antonio Santos-Flórez¹ and Maurice de Koning^{1,2,*}

¹*Instituto de Física “Gleb Wataghin”, Universidade Estadual de Campinas, UNICAMP, 13083-859, Campinas, São Paulo, Brazil*

²*Center for Computing in Engineering & Sciences, Universidade Estadual de Campinas, UNICAMP, 13083-861, Campinas, São Paulo, Brazil*

(Dated: September 3, 2022)

I. INTERACTIONS MODELS

We consider the set of purely repulsive interaction models detailed below. In all cases, ϵ_{ij} and σ_{ij} are energy and length scales associated with the interactions between particles i and j , and r_{ij} is the distance between them. In all simulations we fix the energy scales of the interactions between particles of the same species to be $\epsilon_{AA} = 100\epsilon$ and $\epsilon_{BB} = 200\epsilon$, respectively, whereas the energy scale ϵ_{AB} for interactions between A and B is variable. The length scale is chosen to be the same for all interaction types, i.e., $\sigma_{AA} = \sigma_{BB} = \sigma_{AB} = \sigma$.

A. Uhlenbeck-Ford

The interactions described by the purely repulsive Uhlenbeck-Ford (UF) model¹⁻⁴ are characterized by a logarithmic divergence at zero separation and belong to the class of so-called ultrasoft potentials⁵, which have been shown to be useful in the description of the effective interactions between star-polymer particles⁶⁻⁹. Specifically, the UF model is defined by the potential-energy function

$$u(r_{ij}) = -\epsilon_{ij} \ln(1 - e^{-r_{ij}^2/\sigma_{ij}^2}). \quad (1)$$

The cut-off for the interaction calculation is set at $r_c = 4\sigma$.

B. Inverse fourth-power and sixth-power laws

The potential-energy functions describing the inverse fourth (IPL4) and sixth-power (IPL6) laws¹⁰ are given by

$$u(r_{ij}) = \epsilon_{ij} \left(\frac{\sigma_{ij}}{r_{ij}} \right)^n, \quad (2)$$

with the cut-offs for the interaction calculation set at $r_c = 6\sigma$ and $r_c = 4\sigma$, respectively, for the IPL4 and IPL6 models.

C. Weeks-Chandler-Andersen

The Weeks-Chandler-Anderson (WCA) model¹¹ is defined by the repulsive part of the Lennard-Jones (LJ) potential energy function, shifting the LJ function such that the minimum value corresponds to zero, and truncating it for distances beyond that of its minimum at $r = 2^{1/6}\sigma$. For the binary mixture, the WCA force field is defined as

$$u(r_{ij}) = \begin{cases} 4\epsilon_{ij} \left[\left(\frac{\sigma_{ij}}{r_{ij}} \right)^{12} - \left(\frac{\sigma_{ij}}{r_{ij}} \right)^6 \right] + \epsilon_{ij}, & \text{if } r \leq 2^{1/6} \sigma_{ij} \\ 0, & \text{otherwise.} \end{cases}$$

D. Gaussian core

The Gaussian core model for the binary system is defined as¹²

$$u(r_{ij}) = \epsilon_{ij} \exp(-r_{ij}^2/\sigma_{ij}^2). \quad (3)$$

E. Behavior at the origin

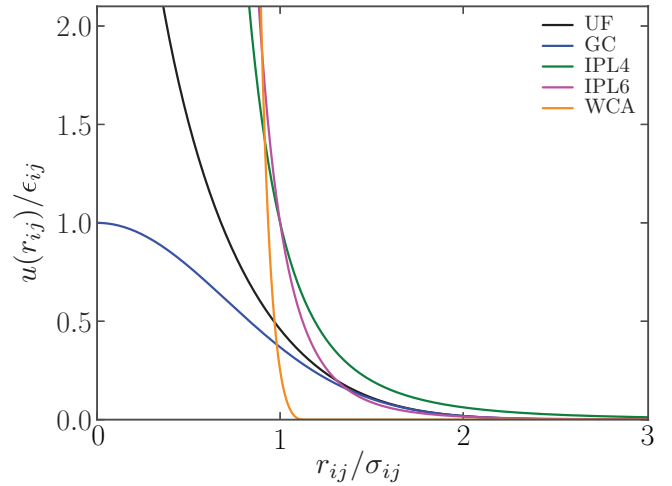


Figure S1. (Color online) Graphs of considered repulsive pair potentials.

The main difference between these models is their behavior near the origin, as can be seen in Fig. S1. The UF,

IPL4, IPL6 and WCA models all diverge at the origin, yet at different rates. Whereas the UF model diverges only logarithmically, the IPL4, IPL6 and WCA force fields diverge as r^{-4} , r^{-6} and r^{-12} , respectively. The GC, on the other hand, does not diverge as $r \rightarrow 0$, reaching a constant value at zero slope.

II. INSTABILITY WITH RESPECT TO COMPOSITION FLUCTUATIONS FOR THE UF MODEL

Depending of the magnitude of the inter-species energy scale, the random initial configuration for the UF model is unstable with respect to composition fluctuations, giving rise to the unmixing transition. This is illustrated in Fig. S2, which shows the mean energy obtained for 5000 random initial conditions as a function of composition at a reduced density $\rho^* = 1$ for a number of different values for ϵ_{AB} . For $\epsilon_{AB} \lesssim 140$, the energies are convex functions of the particle-type fraction, implying that the mixtures in these cases are stable. For $\epsilon_{AB} \gtrsim 150$, on the other hand, the curves have become concave for any composition, implying that mixtures in any proportion of A and B species are unstable¹³, giving rise to an unmixing transition.

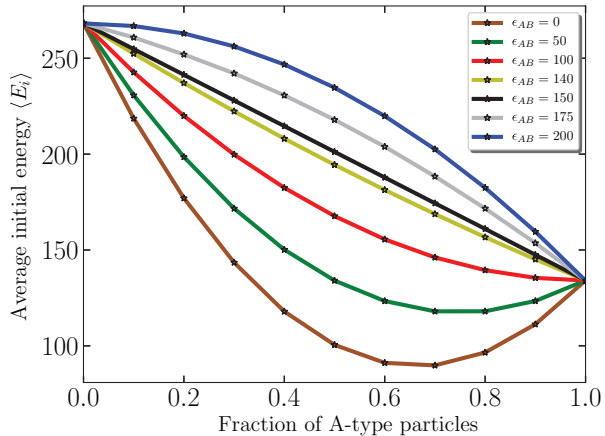


Figure S2. (Color online) Mean initial energy as a function of the A -particle fraction for different values of ϵ_{AB} .

III. DETERMINATION OF GRAIN-SIZE DISTRIBUTION

To assess the grain-size statistics we employ the grain-tracking algorithm (GTA) developed by Panzarino and Rupert,¹⁴ which allows one to identify and determine the size of grains with face-centered cubic (fcc) or body-centered cubic (bcc) crystal structures. Since the rock-salt (B1) crystal structure for the binary system is composed of two interpenetrating fcc lattices, each occupied

by one of the species, the grains can be identified by applying the algorithm to configurations in which only one of the species is considered. Visual inspection¹⁵ indeed shows that the results for the grain structure are qualitatively independent of the particular species used in the analysis, as evidenced in Fig. S3.

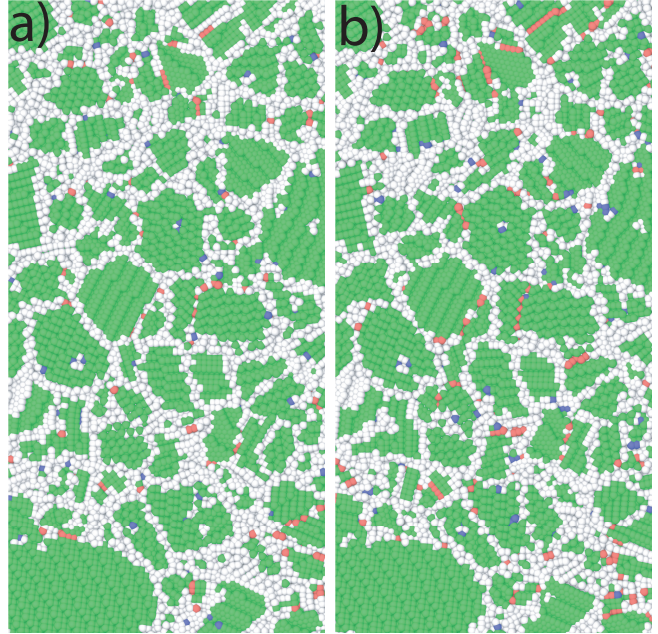


Figure S3. (Color online) (a) and (b) display the grain structures as visualized by considering, respectively, species A and B , individually. The different colors correspond to distinct local symmetries: fcc (green), bcc (blue) and hcp (red). Particles shown in white represent those in disordered surroundings.

Moreover, also in quantitative terms does the GTA give essentially identical grain statistics for both particle species, as shown in Fig. S4. It displays the rank-size graphs^{16,17} of the grains identified by the GTA for species A and B , respectively. Specifically, the graphs plot the rank of each grain in terms of its size as a function of grain size, such the largest and smallest grains are ranked first and last, respectively. Both distributions are very similar, in particular for the larger grain sizes. Indeed, on the log-log scale, both plots display linear behavior for grain sizes larger than ~ 4000 particles, implying that the distribution of grain size k follows a power-law of the form

$$p(x) = Ck^{-\alpha}, \quad (4)$$

where α is the exponent and C is a normalization constant. From the rank-size data we can estimate the exponent according to the maximum-likelihood estimator for discrete variables^{16,17}

$$\alpha = 1 + n \left[\sum_{i=1}^n \ln \frac{k_i}{k_{\min} - \frac{1}{2}} \right]^{-1}, \quad (5)$$

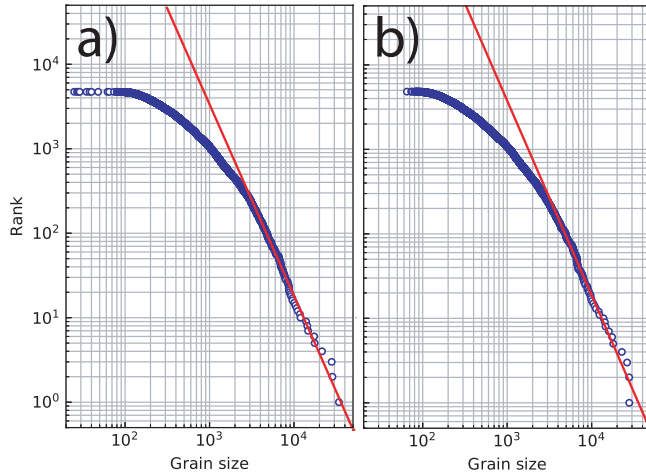


Figure S4. (Color online) Log-log representation of the rank-size graphs of the number of particles in the grains identified by the GTA algorithm for, (a), species *A* and, (b), species *B*. Each circle corresponds to one of the grains identified by the GTA. Red lines represent guides to the eye obtained by linear regression for the group of the 125 largest grains.

where the k_i are the grain sizes measured by the GTA, k_{\min} is the smallest value of x for which power-law behavior is observed and the index i runs over all grains with sizes equal to or larger than k_{\min} . The associated statistical error is

$$\sigma = \frac{\alpha - 1}{\sqrt{n}}. \quad (6)$$

The data in the graphs of Fig. S2, selecting $k_{\min} = 4275$ so as to take into account the ~ 125 largest grains, gives statistically equal exponents for both species, namely $\alpha = 3.3 \pm 0.2$ and $\alpha = 3.2 \pm 0.2$, for *A* and *B*, respectively.

* dekonig@if.unicamp.br

- ¹ G. Uhlenbeck and G. Ford, "Studies in statistical mechanics," in *Series in physics*, v. 1, edited by J. de Boer and G. Uhlenbeck (North-Holland Publishing Company, 1962) Chap. The development of linear graphs with applications to the theory of the virial development of the properties of gases, p. 182.
- ² R. Paula Leite, R. Freitas, R. Azevedo, and M. de Koning, *J. Chem. Phys.* **145**, 194101 (2016).
- ³ R. Paula Leite, P. A. Santos-Flórez, and M. de Koning, *Phys. Rev. E* **96**, 032115 (2017).
- ⁴ R. Paula Leite and M. de Koning, *Comput. Mater. Sci.* **159**, 316 (2019).
- ⁵ C. N. Likos, N. Hoffmann, H. Löwen, and A. A. Louis, *J. Phys.: Condens. Matter* **14**, 7681 (2002).
- ⁶ C. N. Likos, H. Löwen, M. Watzlawek, B. Abbas, O. Jucknischke, J. Allgaier, and D. Richter, *Phys. Rev. Lett.* **80**, 4450 (1998).

- ⁷ M. Watzlawek, C. N. Likos, and H. Löwen, *Phys. Rev. Lett.* **82**, 5289 (1999).
- ⁸ A. Jusufi, M. Watzlawek, and H. Löwen, *Macromolecules* **32**, 4470 (1999).
- ⁹ C. N. Likos, *Phys. Rep.* **348**, 267 (2001).
- ¹⁰ S. Kambayashi and Y. Hiwatari, *Phys. Rev. A* **46**, 1014 (1992).
- ¹¹ J. D. Weeks, D. Chandler, and H. C. Andersen, *J. Chem. Phys.* **54**, 5237 (1971).
- ¹² F. H. Stillinger, *J. Chem. Phys.* **65**, 3968 (1976).
- ¹³ D. A. Porter, K. E. Easterling, and M. Sherif, *Phase Transformations in Metals and Alloys (Revised Reprint)* (CRC Press, 2009).
- ¹⁴ J. F. Panzarino and T. J. Rupert, *JOM* **66**, 417 (2014).
- ¹⁵ A. Stukowski, *Model. Simul. Mater. Sci. Eng.* **18**, 015012 (2010).
- ¹⁶ M. Newman, *Contemp. Phys.* **46**, 323 (2005).
- ¹⁷ A. Clauset, C. Shalizi, and M. Newman, *SIAM Rev.* **51**, 661 (2009).